applied sciences

MDPI

Article

The Use of Volcanic Powder as a Cement Replacement for the Development of Sustainable Mortars

Viviana Letelier [1,*], José Marcos Ortega [2], Rosa María Tremiño [2], Bastián I. Henriquéz-Jara [1], Ivo Fustos [1], Teresa Real-Herraiz [3], Giacomo Moriconi [4], Miguel Ángel Climent [2] and Isidro Sánchez [2]

1 Departamento de Obras Civiles, Universidad de la Frontera, Av. Fco. Salazar, Temuco 01145, Chile; b.henriquez01@ufromail.cl (B.I.H.-J.); ivo.fustos@ufrontera.cl (I.F.)
2 Departamento de Ingeniería Civil, Universidad de Alicante, Ap. Correos 99, 03080 Alacant/Alicante, Spain; jm.ortega@ua.es (J.M.O.); rmta2@alu.ua.es (R.M.T.); ma.climent@ua.es (M.Á.C.); isidro.sanchez@ua.es (I.S.)
3 Instituto de Matemática Multidisciplinar, Universidad Politécnica de Valencia, Camino de Vera s/n, 46022 Valencia, Spain; tereaher@upv.es
4 Department of Science and Engineering of Matter, Environment and Urban Planning, Università Politecnica delle Marche, Via Brecce Bianche, 60131 Ancona, Italy; g.moriconi@univpm.it
* Correspondence: viviana.letelier@ufrontera.cl; Tel.: +56-45-2325681

Received: 30 December 2019; Accepted: 18 February 2020; Published: 21 February 2020

Abstract: Currently, reduction of environmental effects of the cement industry is an issue of global interest and one of the alternatives is to replace clinker with additions such as volcanic powder. The purpose of this work is to study the influence of up to 400 hardening days of volcanic powder, obtained from the last eruption of the Calbuco volcano (Chile), on the pore structure, mechanical performance, and durability-related properties of mortars which incorporate up to 20% volcanic powder as a substitution for clinker. In addition, an evaluation of greenhouse gases emissions was performed in order to quantify the possible environmental benefits of incorporating the volcanic powder in the mortars. The results obtained indicated that mortars with contents of 10% and 20% of volcanic powder had adequate service properties and improved all durability-related properties overall as compared with those noted for ordinary Portland cement. Additionally, the use of up to 20% volcanic powder makes it possible to reduce the CO_2 emissions of mortars by almost 20%, demonstrating the advantages of incorporating this addition in mortars.

Keywords: volcanic powder; Calbuco volcano; sustainability; microstructure; durability; mechanical properties; impedance spectroscopy

1. Introduction

The great development of the construction industry in recent decades has entailed a worldwide rise in both the demand for raw materials and the production of a large quantity of construction and demolition wastes. This has produced inevitable environmental problems around the construction industry [1]. As a solution for reducing the effects of these issues, many countries have created sustainable development programs in which the use of recycled materials has a major importance [2].

Concrete is one of the most popular construction materials in the world. As a result, many studies have focused on reducing the environmental damages associated with its manufacturing. Several investigations have been based on one solution which is related to the study of the effects of substituting different concrete constituents with reused materials [3–7].

The high levels of CO_2 emissions generated by the cement industry, estimated to be 5% and 7% of the total worldwide emissions [8–11] have motivated the cement industry to tackle the important challenges of reducing raw materials, energy demands, and CO_2 emissions.

According to the study performed by Stafford and Raupp-Pereira [12], within the service life of cement, the transport stage, followed by the production of fossil fuels and clinkering, were mostly responsible for the environmental impact of this industry. These processes combined were the origin of approximately 70% of equivalent CO_2, as well as 90% of equivalent CFC-11 (trichlorofluoromethane) gases of cement production.

In light of this information, to substitute part of cement with a supplementary material derived from residues represents one of the most suitable ways to reduce the environmental negative effects of concrete [13–17]. This would entail a reduction of energy consumption, costs, and volume of wastes produced [18].

The research works conducted on the possibility of using volcanic powder (VP) in mortars, concretes, and cement-based materials in general, concluded that VP accomplishes the prescriptions of ASTM C618 standard regarding its use as a pozzolanic material [19]. However, the capacity of an ash or powder material for replacing Portland cement partly depends on its pozzolanic activity and, in turn, is related to the quantity of silica reactive and the amorphous phases present in the ash [20].

Generally, on the one hand, when the cement replacement percentage exceeds 10%, there are more significant losses in compressive strength, which is why the general recommendation is to use up to a maximum of 15% to 20% VP as a cement replacement, in order to limit losses in strength [21,22]. According to Kupwade-Patil et al. [23], this could be explained in relation to the presence in VP materials of diopside, deforsterite, and periclase that are related to phases based in magnesium, which entailed the appearance of M-S-H and other associated crystalline phases. Overall, they are considered as phases with lower strength as compared with C-S-H and C-A-S-H gels. Furthermore, high percentages of VP produce a greater porosity because of the presence of higher concentrations of CaO and Fe_2O_3 [24], also resulting in a reduction in the strength.

On the other hand, it has been indicated that using low contents of VP could be positive in terms of durability of concrete, since it produces materials more resistant to the attack of seawater [25], carbonation, and chloride ion penetration [26]. Regardingthe economic benefits of using VP in cement-based materials, they depend on the distance between the deposit of volcanic materials and the cement manufacturingfacility, the required grinding, and the reduction of the costs related to the transport of volcanic material to landfills [27].

The main aim of this research is to study the influence of the addition of VP, obtained from the last eruption of the Calbuco volcano (Chile), on the pore structure, mechanical performance, and durability of mortars which incorporate 10% and 20% of VP as a substitution for clinker, as compared with reference mortars which were prepared with ordinary Portland cement without incorporating additions. The development of the pore network of the studied materials was analyzed using the mercury intrusion porosimetry and impedance spectroscopy techniques. Regarding the durability-related properties, the non-steady state chloride migration coefficient was studied, as well as the steady-state diffusion coefficient obtained from sample's resistivity. In addition to this, both compressive and flexural strengths of the mortars were determined. Finally, an evaluation of greenhouse gas emissions was performed in order to quantify the possible environmental benefits of incorporating the volcanic powder in the mortars.

2. Materials and Methods

2.1. Volcanic Powder Characterization

The VP used in this work was obtained from the last eruption of the Calbuco volcano. Calbuco (41°20′ S, 72°37′ W, 2003 m.a.s.l.) is an active stratovolcano which belongs to the southern Andes, sited among Ensenada and Puerto Montt, in Chile. The last subplinian eruption happened on 22 and 23 April 2015, with a total volume of tephra fall deposits calculated to be 0.27 km^3. Analyses of the erupted debris revealed the presence of porphyritic basaltic andesite (~55% by weight of SiO_2) [28]. On the one hand, the fallout mostly affected the northeast area of the volcano. On the other hand, the

finest ashes were deposited mainly in southern Chile and Argentinean Patagonia. The analysis of the size distribution of particles showed fractions between 3 and 350 μm, variably distributed as a function of the distance from the origin [29].

The material used in this study was previously sifted and the VP particles used were less than 75 μm.

The chemical analysis, determined with X-ray fluorescence (XRF), and the VP physical properties are listed in Table 1. According to the table, the main components of VP are silica, aluminum, and iron. The particle size distribution is depicted in Figure 1.

Table 1. Physical and chemical properties of VP.

Composition	VP
SiO_2	57.76%
Al_2O_3	14.54%
CaO	8.27%
Fe_2O_3	11.00%
SO_3	-
MgO	2.44%
Na_2O	2.41%
K_2O	2.14%
TiO_2	1.42%
Density	2450 kg/m^3
Blaine surface area	285 m^2/kg

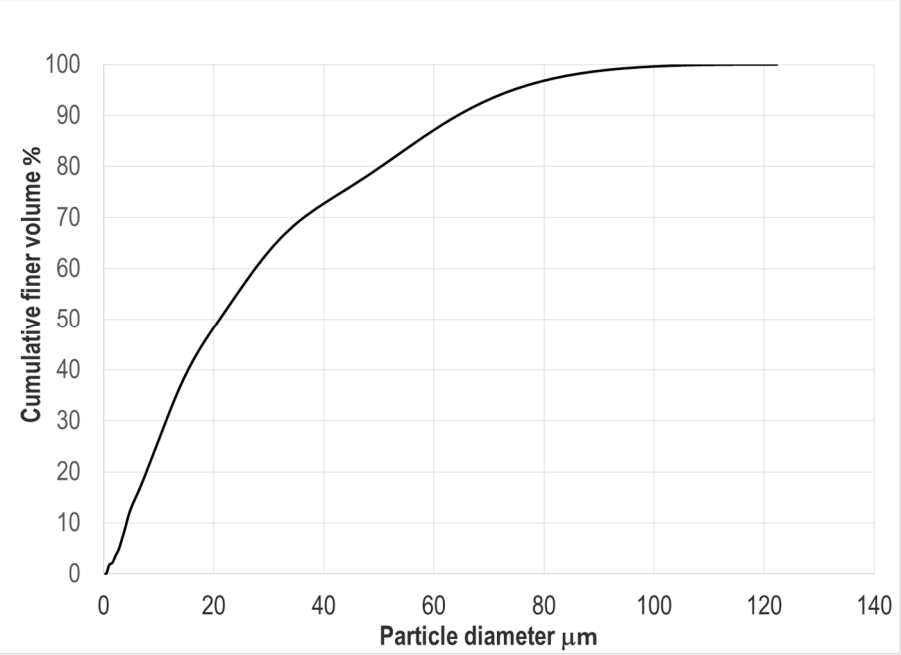

Figure 1. Grain size distribution of volcanic powder (VP).

The scanning electron microscopic (SEM) analysis of the VP appears in Figure 2, and it was performed using a scanning electron microscope model Hitachi S3000N (Hitachi, Krefeld, Germany). The analysis showed that the particles of VP are irregular showing very smooth surfaces, which is consistent with the low surface area shown in Table 1. In addition, Figure 3 represents the energy-dispersive X-ray (EXD) spectroscopy for the VP obtained by SEM, which is in agreement with the results of the chemical analysis noted in Table 1.

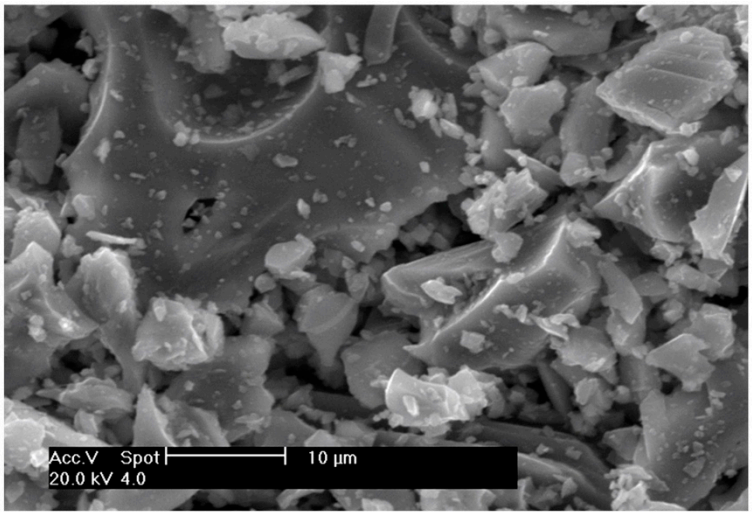

Figure 2. SEM micrograph of volcanic powder.

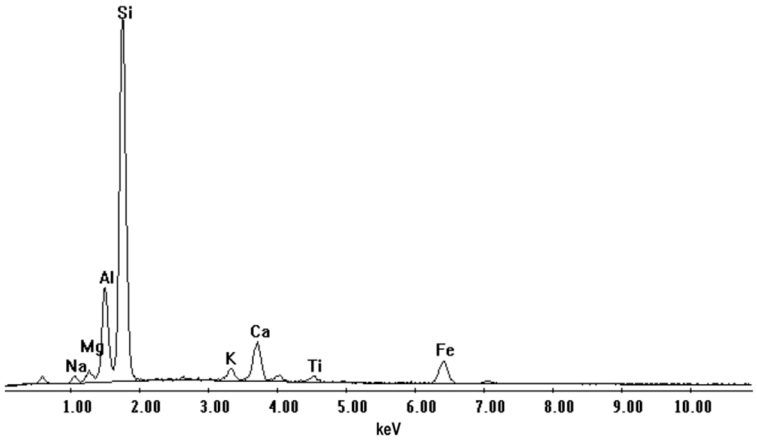

Figure 3. EDS analysis of volcanic powder.

2.2. Sample Preparation and Environmental Conditions

Three kinds of cement mortars have been analyzed in this study, a control mortar prepared with ordinary Portland cement CEM I 42.5 R (CEM I) and accomplishing the Spanish and European standard UNE-EN 197-1 [30] requirements, and two mortars with a 10% and 20% replacement of the abovementioned commercial ordinary Portland cement CEM I by volcanic powder (named VP10 and VP20, respectively). In all the mortars, a water cement ratio of 0.5 and an aggregate cement ratio of 3:1 were used. Fine aggregates are siliceous with a particle size that complied with the stipulations of the UNE-EN 196-1 [31] standard.

For the mechanical strength tests, 40 × 40 × 160 mm samples were prepared. For the durability and microstructural tests, cylindrical samples 10 cm in diameter and 15 cm high were used. The cylinders were kept in a chamber at 20 °C and 95% relative humidity for 24 h. After this, the specimens were turned out and sawed into 1 cm and 5 cm high cylinders. Finally, all the samples (prisms and cylinders) were maintained in a room at 20 °C and 100% relative humidity until the testing ages (28, 200, and 400 hardening days).

2.3. Mercury Intrusion Porosimetry

For the analysis of the development of the pore structure of the samples, mercury intrusion porosimetry was used, in spite of its drawbacks [32–34]. The equipment used for performing the tests was a Poremaster-60 GT porosimeter (Quantachrome Instruments, Boynton Beach, FL, USA).

Previously to the test, the samples were oven-dried at 50 °C for 48 h. The results obtained were pore size distribution, total porosity, and percentage of retained Hg at the end of the test. The samples were tested at 28, 100, 200, and 400 days.

2.4. Impedance Spectroscopy

The pore structure evolution of the studied specimens was also analyzed using the non-destructive impedance spectroscopy. This technique shows advantages as compared with others, since it is possible to analyze global information of the pore structure in the samples [35,36], and it is also possible to study the microstructural variations of the same sample throughout the period of time studied [37].

An Agilent 4294A analyzer (Agilent Technologies, Kobe, Japan) was used for the impedance spectroscopy. This device takes capacitance measurements ranging between 10^{-14} and 0.1 F, with a maximum resolution of 10^{-15} F. In this research, circular electrodes (Ø = 8 cm) were used, which consisted of flexible graphite attached to a piece of copper with the same diameter to obtain the impedance spectra. Through these electrodes, frequencies oscillated between 100 Hz and 100 MHz. Regarding the measurement methods, contacting and non-contacting ones were applied [35].

An example of an impedance spectrum that resulted from the measurement of one of the samples studied is depicted in Figure 4a. To validate the measurements, the Kramers–Kronig (K–K) relations were used [38] and a differential impedance analysis was applied to them [39]. According to the plot shown in Figure 4b, it was noted that the measured spectra contained two time constants, revealed by the two maxima in the plot. From this finding, the experimental data can be fitted to the equivalent circuits proposed by Cabeza et al. [36] (see Figure 5a,b), which includes two time constants. These circuits, comprised of various resistances and capacitances, make it possible to relate different characteristics of the pore network of cementitious materials [36]. The R_1 resistance gives information about the percolating pores in the sample, whereas the R_2 resistance provides data related to the pores in general. The C_1 capacitance provides information about the solid fraction of the specimen, and the C_2 capacitance is related to the surface of the pores in contact with the electrolyte that fills the microstructure of the material [36]. Figure 5 shows that the impedance parameters R_2, C_1, and C_2 can be obtained using both contacting and non-contacting methods. In this study, due to their greater accuracy, only the values of the parameters R_2, C_1, and C_2 with the non-contacting method were analyzed. The R_1 resistance can be only determined with the contacting method.

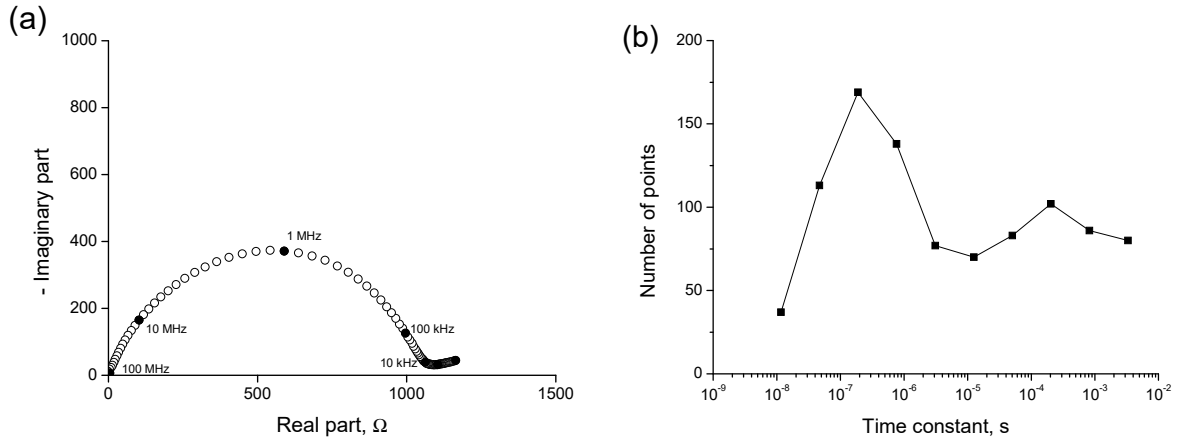

Figure 4. (**a**) Nyquist plot noted for a VP10 specimen at 200 days using the contacting method; (**b**) differential impedance analysis of the impedance spectrum represented in 0a.

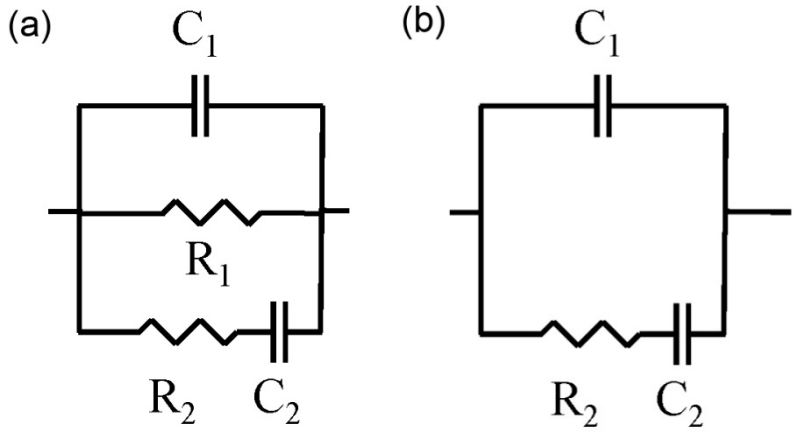

Figure 5. (**a**) Equivalent circuit used for the fitting of the impedance spectra obtained using the contacting method; (**b**) equivalent circuit used for the fitting of the impedance spectra obtained using the non-contacting method.

In this work eight different discs approximately 1 cm thick were analyzed for each mortar type. The changes with time of the impedance parameters over time were recorded up to 400 hardening days.

2.5. Capillary Absorption Test

The capillary absorption analysis was done following the standard UNE 83,982 [40], which follows the Fagerlund method to study the capillarity of cementitious materials, such as the concrete. Prior to the test, the samples were oven-dried completely at 105 °C for 12 h and, then, stored in a container hermetically sealed for 12 h [41], where silica gel was introduced inside. Before the test, the external lateral surface of the samples was sealed with self-adhesive tape, so they would not come in contact with the water [42].

To implement the tests, a flat-based container base was used, on which the samples were positioned as indicated by UNE 83,982 [40]. During the test, the distilled water level was maintained constant at 5 ± 1 mm, keeping the bases of the samples under water throughout. The container was closed during the entire test. The mortars were weighed according to the times established in the standard [40]. The test ended when there was a difference in weight of each sample less than 0.1%, being weighed after a period of 24 h.

The capillary suction coefficient was determined with the following expression:

$$K = \frac{\delta_a \cdot \varepsilon_e}{10 \cdot \sqrt{m}} \text{ with } m = \frac{t_n}{h^2} \quad (1)$$

where K is the capillary suction coefficient (kg/(m^{2}min$^{0.5}$)), δ_a is the density of water (1 g/cm^3), m is the resistance to water penetration by capillary suction (min/cm^2), t_n is the time necessary to reach the saturation (minutes), h is the thickness of the sample (cm), and ε_e is the effective porosity obtained from the next expression:

$$\varepsilon_e = \frac{Q_n - Q_0}{A \cdot h \cdot \delta_a} \quad (2)$$

where Q_n is the weight of the sample at the end of the test (g), Q_0 is the weight of the sample before starting the test (g), and A is the surface of the sample in contact with water (cm^2).

In order to perform this test, for each mortar type, three cylindrical samples 10 cm in diameter and 5 cm thick were studied at 28, 200, and 400 days.

2.6. Steady-State Diffusion Coefficient Obtained from the Resistivity of the Saturated Sample

The electrical resistivity analysis provided data on the connectivity of the pores in the mortars, as well as data to determine the chloride diffusion coefficient (D_S) [43]. In this study, resistivity was calculated using the R_1 impedance spectroscopy values, determined in cylindrical samples 10 cm in diameter and 5 cm thick. According to Section 2.4, the R_1 impedance resistance is associated to the pores that cross the specimen [35], and therefore is equivalent to its electrical resistance [41]. For this test, the samples were saturated for 24 h following the procedure indicated in ASTM C1202 [44] and after measuring the resistance R_1, they were also utilized for conducting the forced migration tests. To calculate the steady-state ionic diffusion coefficient, the following expression was used [33]:

$$D_S = \frac{2 \times 10^{-10}}{\rho} \quad (3)$$

where D_s is the chloride steady-state diffusion coefficient through the sample (m^2/s) and ρ is the electrical resistivity of the specimen ($\Omega \cdot m$).

For each cement type, three different samples were tested at 28, 200, and 400 days.

2.7. Forced Migration Test

The forced chloride migration test was done following the standard NT Build 492 [45]. For this test, samples saturated in distilled water were used. The result of this test is the non-steady-state chloride migration coefficient (D_{NTB}). For each mortar sample, three cylindrical samples 10 cm in diameter and 5 cm high were used at 28, 200, and 400 hardening days.

2.8. Mechanical Strength Test

The compressive and flexural strengths were tested on each mortar type according to the UNE-EN 196-1 standard [31], using a compression testing machine model Servosis MEM-101/10A (Servosis, Madrid, Spain). Three different prismatic samples with sizes of $4 \times 4 \times 16$ cm were used at 28, 200, and 400 hardening days.

2.9. Evaluation of Greenhouse Gas (GHG) Emissions

Equation (4) has been proposed to calculate the total greenhouse gas emissions (GHG_{tot} in $kgCO_2/ton$) in relation to the production and transport of the mortars studied:

$$GHG_{tot} = GHG_{raw} + GHG_{sub} \quad (4)$$

where: $GHG_{raw}(kgCO_2/ton)$ is the greenhouse gases emitted by the original materials and is calculated according to Equation (5):

$$GHG_{raw} = \sum_{f \in CV} \sum_{k=1}^{n} P_k \cdot (1 - R_k) \cdot \theta_k^f \quad (5)$$

$GHG_{sub}(kgCO_2/ton)$ is the greenhouse gases of the replacement materials and is calculated according to Equation (6):

$$GHG_{sub} = \sum_{f \in CV} \sum_{k=1}^{m} P_k \cdot R_k \cdot \theta_k^f \quad (6)$$

where n represents the total original raw materials (in the control mortar), m represents the total replacement raw materials, f represents the life cycle stages (CV) to be analyzed, and P_k is the relation between the raw material k and the total mass of the material (kg/kg). In the case of the replacement raw materials, it is the relation of the original raw materials and total mass of the material. R_k is the replacement ratio (where replaced) or added ratio (where a replacement) of the raw material k. θ_k^f is the CO_2 generation ratio of the raw material k in the f phase of the life cycle ($kgCO_2/ton$), in which θ_k^p

is the amount of emissions associated with the production phase of the raw material k and θ_k^t is the amount of emissions associated with the transport of the raw material k, which is calculated as follows:

$$\theta_k^t = d_k \cdot G \quad (7)$$

where d_k represents the distance thatthe raw material is transported (km) and G represents the emissions associated with transporting one ton per kilometer ($kgCO_2/(ton \cdot km)$).

The factors and results related to the CO_2 emissions (in $kgCO_2$ per ton of mortar) and the embodied energy for the mortars analyzed, derived from the previously explained procedure, are shown in Table 2. The factors corresponding to the cement were taken from the "Inventory of Carbon and Energy" [46]. For the sand and volcanic powder, the energy consumed in the sifting process and the associated emissions were estimated [47]. In order to calculate the emissions emitted when transporting the raw materials, the database for Conversion Factors for Greenhouse Gases from the UK government was considered [48].

Table 2. Factors used to calculate the greenhouse gas (GHG) emissions.

Raw Material	P_k	R_k	θ_k^p	G	d_k	θ_k^t	Embodied Energy
	$\frac{kg}{kg}$	%	$\frac{kgCO_2}{ton}$	$\frac{kgCO_2}{ton \cdot km}$	km	$\frac{kgCO_2}{ton}$	$\frac{MJ}{kg}$
Cement ($k = c$)	0.273	0 10 20	830	0.142	50	7.089	4.6
VP ($k = VP$)	0.273	0 10 20	6	0.142	50	7.089	0.0045
Sand ($k = s$)	0.818	0	14	0.142	100	14.177	-

Then, to compare the sustainability of the material used (volcanic powder) and the original one (cement), the SUB-RAW Index was applied [49], which is defined as follows:

$$\text{SUB} - \text{RAW index} = \left[\log(EE_{raw}) - \log(EE_{sub}) + \log\left(\theta_c^p\right) - \log\left(\theta_{VP}^p\right)\right]/2 \quad (8)$$

where EE_{raw} is the embodied energy of the cement (replaced material) (MJ/kg) and EE_{sub} is the embodied energy of the replacement material (MJ/kg).

For this index, which can take values between −9 and 9, the more positive the value, the greater is the relative sustainability of the analyzed material.

3. Results and Discussion

3.1. Mercury Intrusion Porosimetry

The results discussed here are the total porosity, the retained Hg at the end of the experiment, and the pore size distribution of the cement pastes. The pore size distribution was analyzed considering the next diameter intervals: <10 nm, 10100 nm, 100 nm to 1 µm, 110 µm, 10 µm to 0.1 mm, and >0.1 mm.

The total porosity results (Figure 6) showed that the porosity increases as the percentage of VP increases. On the one hand, the VP10 cases showed porosities very similar to the reference cement for all ages; however, for the VP20 cases, the porosities were greater than those presented by CEM I. On the other hand, the porous structure (Figure 7) of the specimens with VP was more refined for both the VP10 and VP20 as the curing time increased, showing their greatest volume of finer pores at 400 days. This delay in the microstructure development could be due to the greater time needed to initiate the pozzolanic reactions of the volcanic powders than for CEM I hydration. In addition, the higher

refinement of the pores with age presented by the samples with VP10 and VP20 as compared with the CEM I specimens, is indicative of the formation of new solid phases produced by the abovementioned pozzolanic reactions of volcanic powders.

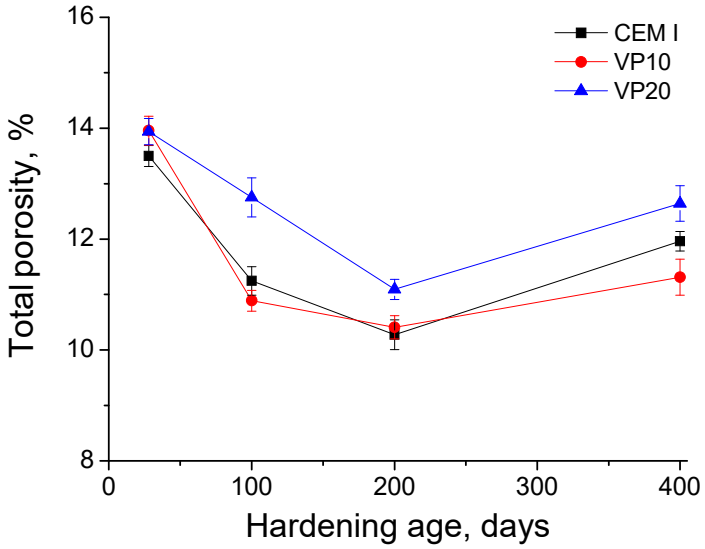

Figure 6. Total porosity of the mortars studied.

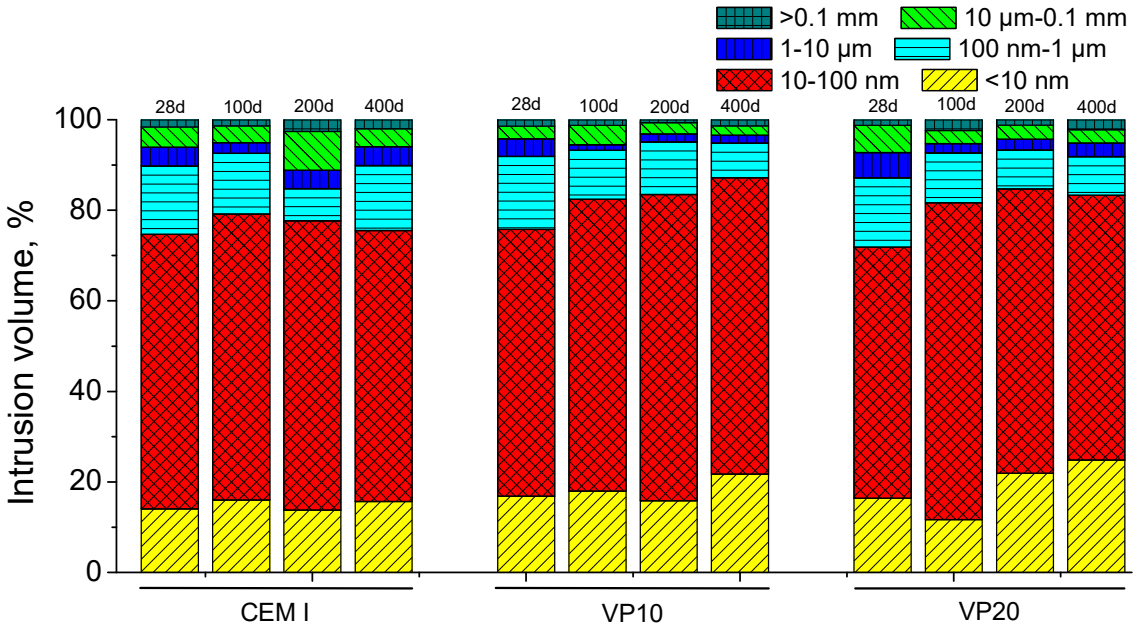

Figure 7. Pore size distribution of the mortars studied.

The percentage of Hg retained in the sample at the end of the test (Figure 8) gives data related to the tortuosity of the microstructure. As can be observed, at 400 hardening days, the values of Hg retained obtained for VP mortars were greater than those noted for the CEM I specimens, which suggests a higher pore network refinement, coinciding with the pore size distributions previously described and discussed.

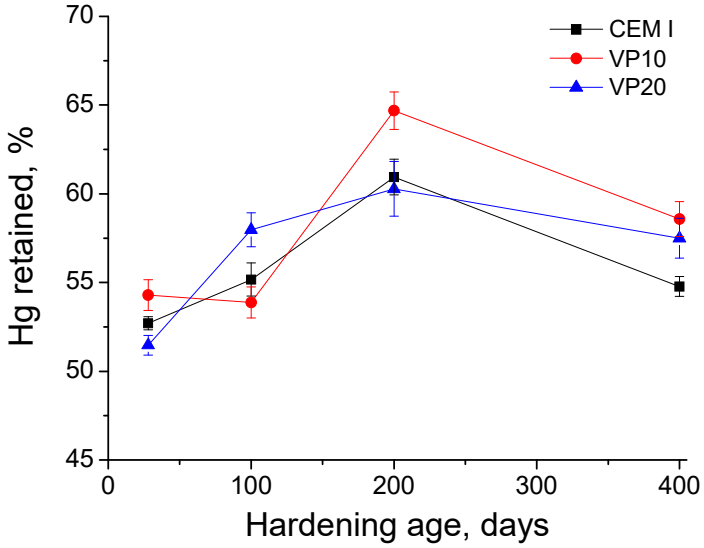

Figure 8. Percentage of mercury retained at the end of mercury intrusion porosimetry test for the mortars analyzed.

3.2. Impedance Spectroscopy

The R_1 and R_2 resistances have a relation with the electrolyte that fills the pores in the specimen [35]. The changes in the resistance value could come from the changes in the sizes of the pores or the pores drying [35,37]. Figures 9 and 10 present the results of the R_1 and R_2 resistances, respectively, for mortars with CEM I, VP10, and VP20. For all the series, the R_1 resistances increased over time. In the case of the series with VP10, at short times the R_1 values were similar to those noted for CEM I. Nevertheless, from around 28 days, the R_1 resistances presented lower values than the reference series with CEM I, a trend that changes after 200 days, where the increase ratio of the VP10 series increased over CEM I, which means that after 270 days the VP10 series presented slightly higher values than the series with CEM I. Otherwise, the series with VP20, at short hardening times the R_1 values were similar to those of the CEM I series. In spite of that, from about 28 days, the R_1 resistance began to rise to a greater ratio than the series with CEM I, similar to the VP10 series, from 200 days the growth ratio increased markedly as compared with the CEM I series.

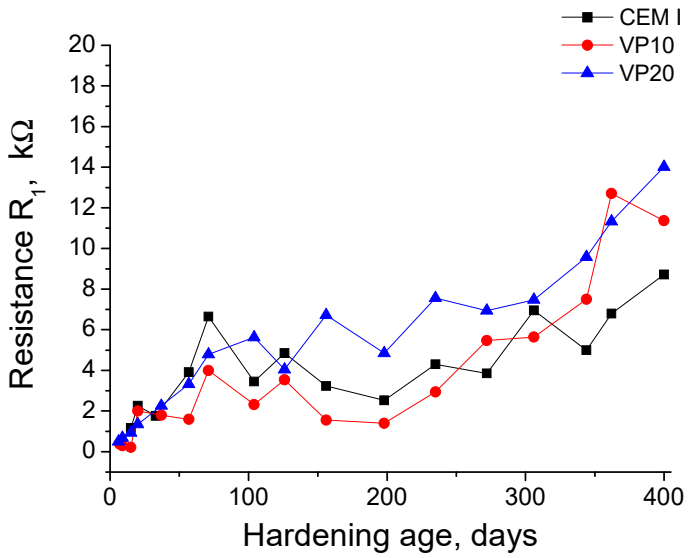

Figure 9. Impedance spectroscopy R_1 resistance for the mortars studied.

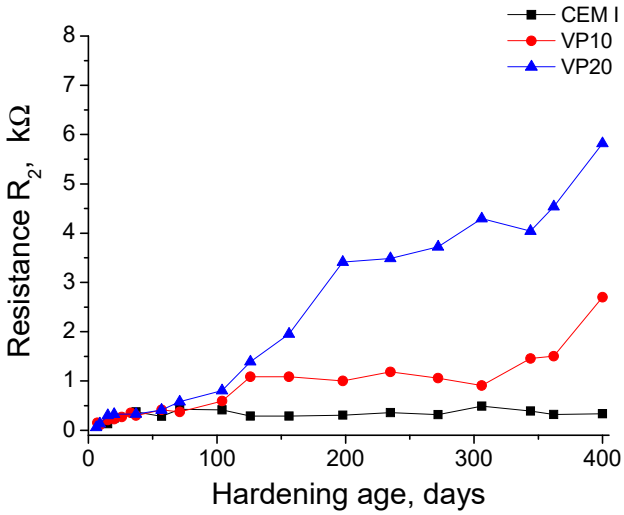

Figure 10. Impedance spectroscopy R_2 resistance for the mortars studied.

In the case of the R_2 resistance, the resistances associated with the reference series (CEM I) remained practically constant over time; however, the R_2 resistance of the series with VP had a higher growth ratio than the series with CEM I, which was more noticeable beyond 50 curing days. Although both series with VP presented higher values than the CEM I series, the increase in R_2 resistance was much greater in the VP20 series than the VP10 series.

At longer ages, the higher resistances noted for the samples with VP could be related to their fine microstructure, which showed a progressive closing of their microstructure, likely linked to the development of pozzolanic reactions, as also shown by the pore distribution size results. In light of this, the results of the R_1 and R_2 resistances would corroborate the pore refinement of the microstructure of mortars with VP, previously observed by mercury intrusion porosimetry, therefore, the the R_1 and R_2 resistances results would be consistent with those noted for pore size distributions and retained Hg at the finish of the test.

The results of the C_1 capacitance observed for the CEM I, VP10, and VP20 series are shown in Figure 11. The C_1 capacitance gives data about the solid fraction of the specimens. Therefore, this parameter should rise when the formation of solids occurs as a consequence of the development of clinker hydration and VP pozzolanic reactions. This capacitance is not dependent on the pore diameters distribution. Overall, the C_1 capacitance remained constant after 50 curing days in all the samples studied. The VP10 series showed values very similar to those of the series with CEM I, and their long-term values were slightly higher when VP was used as compared with the samples with CEM I. In the case of the series with VP20, the values were slightly higher than those obtained with VP10 and CEM I. These C_1 results would be in agreement with the relatively similar values of total porosity obtained for all the mortars tested (see Figure 6).

The evolution of the C_2 capacitance over time for all the series analyzed is represented in Figure 12. The C_2 capacitance is linked with the surface of the pores which are contacting with the electrolyte held in the pore network of the material and has a relation to the formation of the C-S-H gel layer, which progressively fills the pores [37]. These products are formed on the surface of the pores, producing rough structures that increase the specific pore surface and tortuosity of the microstructure. This increase in the specific pore surface entails a rise in the solidelectrolyte interface, which results in greater C_2 capacitance values. Overall, at early ages, a rise of this parameter has been noted for all the series studied, which is linked to an important production of solids in the existing pores surface due to the development of clinker hydration and VP pozzolanic reactions. These new phases progressively refine the pore network. From approximately 100 curing days, practically constant and higher C_2 capacitance values were observed for the samples with VP as compared with the reference mortars. These results, which would be consistent with pore size distributions by intervals, retained Hg, as well

R_1 and R_2 resistances could be due to the progress of pozzolanic reactions of the volcanic powders, which produce the formation of additional C-S-H phases, with respect to clinker hydration, as has already been explained. These C-S-H phases are formed on the existing pore surface, rising it, as well as the tortuosity of the microstructure and the electrolytesolid interface, as the changes with time of this C_2 capacitance suggested.

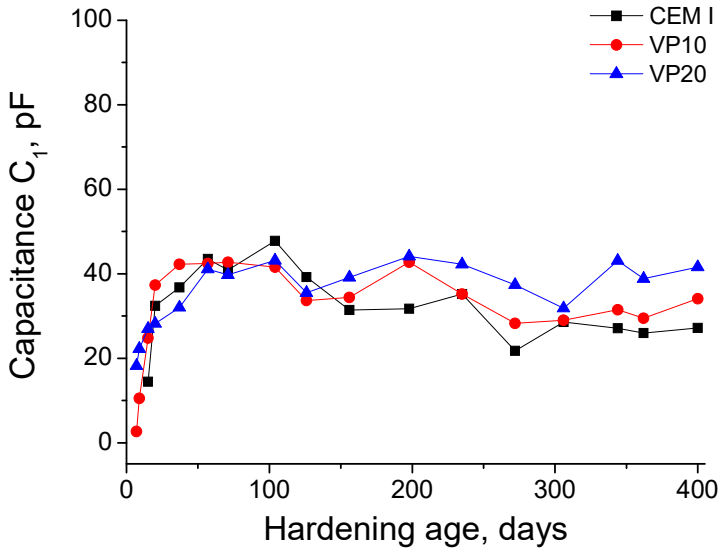

Figure 11. Impedance spectroscopy C_1 capacitance for the mortars studied.

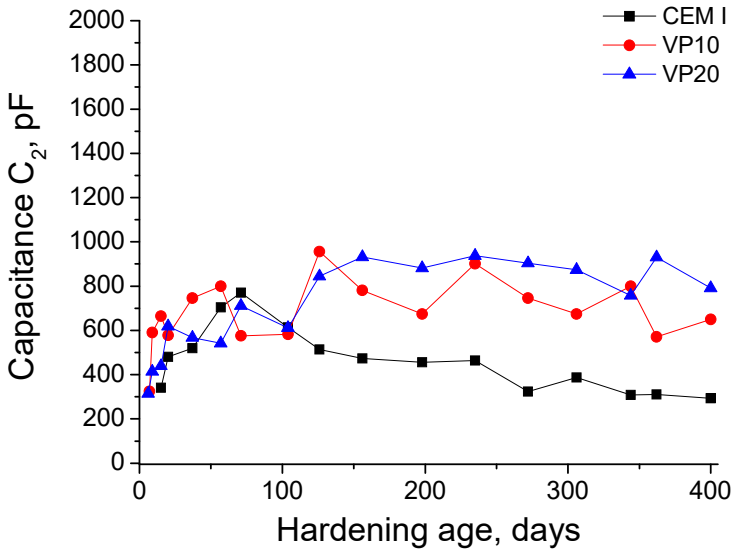

Figure 12. Impedance spectroscopy C_2 capacitance for the mortars studied.

3.3. Capillary Absorption Test

The capillary suction coefficient (K) has a relation with water getting into cementitious materials, and therefore it may be related to the penetration of aggressive elements that can cause steel rebars or pipes to corrode in reinforced concrete. Figure 13 provides the measurements obtained for the different testing ages of the capillary suction coefficient (K) for the specimens with CEM I and VP. In the case of the series with CEM I, the results remained practically constant over time. In the VP10 and VP20 series, however, the coefficient K fell with time for all the mortars, presenting lower long-term values than the CEM I reference series. This reduction with hardening age of this coefficient noted for VP specimens could be related to the development of pozzolanic reactions of this addition. The VP20

series presented greater reductions in time than the VP10 series, which is related to the more refined pore structure generated by the VP20 series in the long term, being in agreement with the results obtained from microstructure characterization tests.

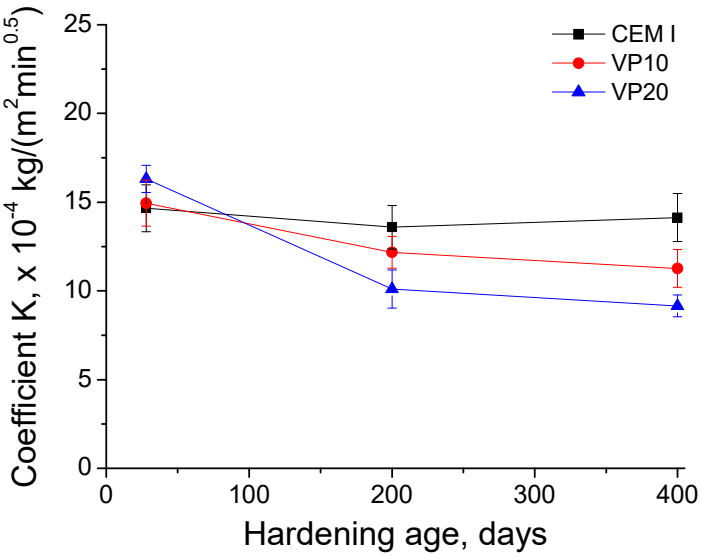

Figure 13. Capillary suction coefficient (K) for the mortars studied.

3.4. Steady-State Diffusion Coefficient Obtained from the Resistivity of the Saturated Sample

The evolution over time of the steady-state chloride diffusion coefficient obtained from the resistivity of the saturated sample is in Figure 14. In the control sample (CEM I), it slightly increased from 28 to 200 curing days, and since then the values stayed practically constant. However, in the samples with VP, the values decreased as the curing days increased. This behavior could be due to the greater refinement of the microstructure for the VP10 and VP20 mortars as compared with CEM I, as the mercury intrusion porosimetry and impedance spectroscopy techniques revealed, whose results were already discussed. This higher refinement of the microstructure of the VP specimens, with greater proportion of pores with smaller diameters, would make the movement of the chloride aggressive ions across the material more difficult, entailing lower values of the diffusion coefficient, which would be in agreement with the results obtained for this parameter.

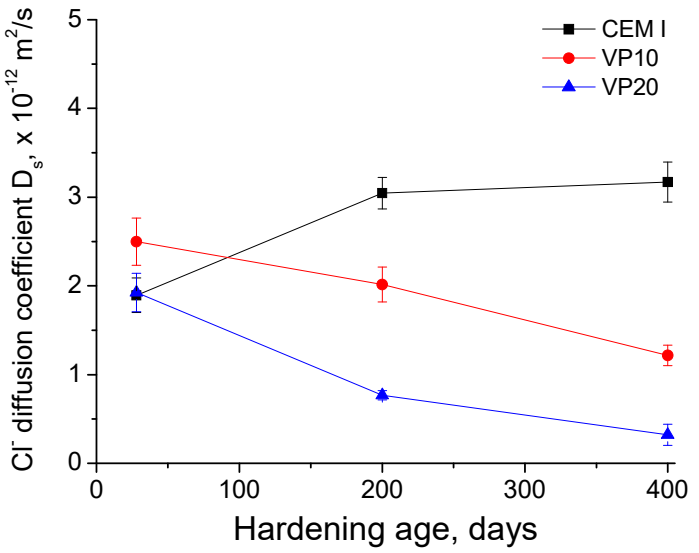

Figure 14. Results of the steady-state chloride diffusion coefficient obtained for the mortars studied.

3.5. Forced Migration Test

Among the durability properties, resistance to cement chloride penetration is of great importance, since chlorides are one of the factors that can cause steel bars and pipes to corrode, mainly for concrete structures located close to the sea or in contact with aggressive waters with high chloride or sulfate contents. In this research, regarding the resistance to cement chloride penetration, the non-steady-state chloride diffusion coefficient was also analyzed (Figure 15). This coefficient showed, from 28 curing days, lower values for the mortars with VP than the CEM I reference mortar. Lower values were observed for the VP20 series than the VP10 series in the long term. They would be consistent with the other results analyzed, especially with those obtained for steady-state chloride diffusion coefficient; this behavior could be due to the long-term refinement of the microstructure mentioned for the VP series as compared with the CEM I samples.

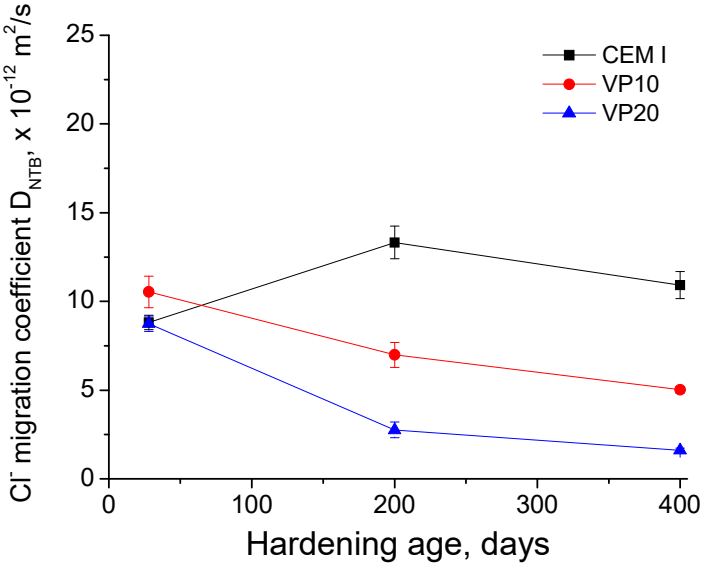

Figure 15. Results of the non-steady-state chloride migration coefficient for the mortars studied.

Generally, the results of the durability-related properties studied in this work were adjusted to those obtained for the characterization of the microstructure. This leads to the conclusion that the use of up to 20% VP makes a significant improvement in the durability properties of mortars.

3.6. Mechanical Properties

The results of compressive strength of the specimens with CEM I and VP appear in Figure 16. As can be observed, all series showed a rise in strength with curing age, which tended to stabilize after 200 curing days. The VP10 series presented a behavior very similar to the CEM I reference series, obtaining a slightly higher value in the long term. However, the VP20 series presented lower values than the CEM I series, not fulfilling the strength objective of 42.5 MPa at 28 curing days, although they accomplished the strength requirement for cements type 32.5 MPa. The differences presented between the densification of the microstructure and compressive strength, as noted in the C_1 capacitance results, stems from the chemical composition of the materials, a fact which could change the compressive strength performance of the material. Regarding the flexural strength (Figure 17), it was slightly higher for the mortars with VP than for the CEM I mortars, not showing any significant strength increases in the study period.

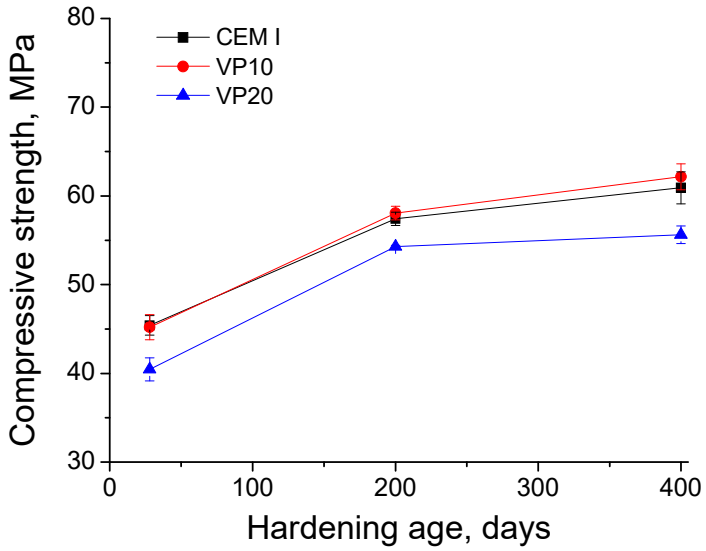

Figure 16. Results of compressive strength for the mortars studied.

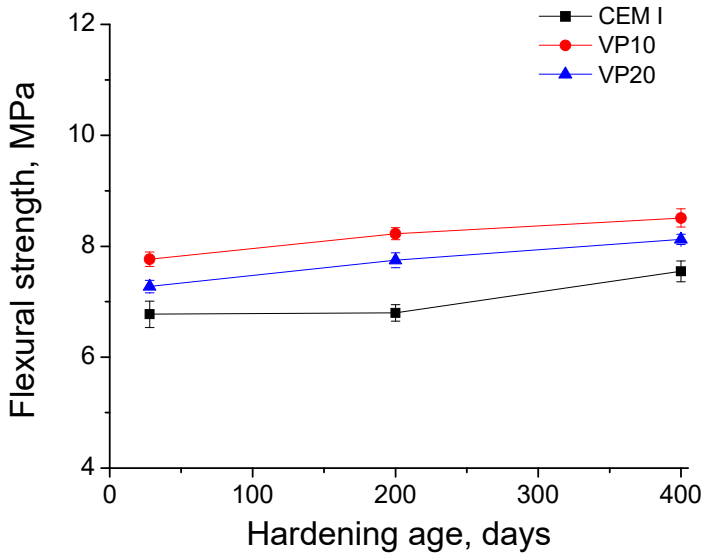

Figure 17. Results of flexural strength for the mortars studied.

3.7. Evaluation of Greenhouse Gas (GHG) Emissions

The emissions associated with the cement were 138 times higher than those associated with VP, which makes the VP emissions insignificant (see Table 2). Therefore, 10% of the original cement mass replaced by VP generated only 0.164 kg/CO_2 per ton. For every 1% of cement replaced by VP, the emissions dropped 0.93% as compared with the control sample. Since the sand was not replaced, it represented a fixed emission for the different mortar samples, nevertheless, which could reduce the transportation distance.

Thus, the greatest emissions reduction in the samples studied was 18.66% for a 20% replacement of CEM I by VP (see Figure 18).

With respect to the SUB-RAW index, a value of 2.57 was obtained, which according to the interpretation by Botempi [49] indicated that the carbon footprint of VP is two orders of magnitude less than that of cement.

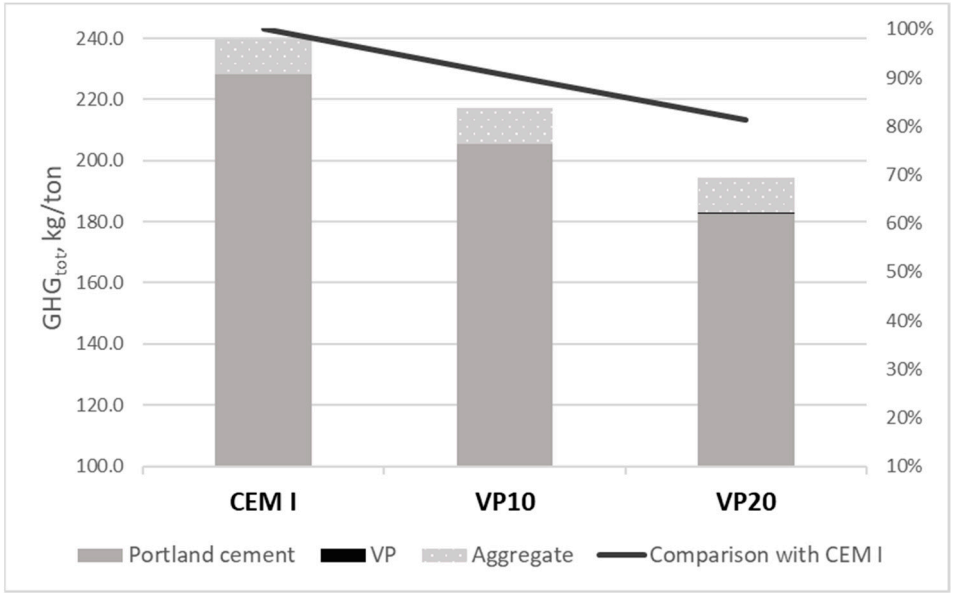

Figure 18. Results of total greenhouse gas emissions (GHG_{tot}) associated with the mortars studied.

4. Conclusions

The main conclusions to be drawn from the previously discussed results can be summarized as follows:

- In all the mortars studied, the pore structure was probably refined as the curing days increased due to the progressive development of clinker hydration and the pozzolanic reactions of the VP;
- Compared to the CEM I mortar, in the mortars with VP a greater refinement of the microstructure was observed, which could be due to the formation of additional solid phases, a result of the pozzolanic reactions of the VP;
- The findings of the non-destructive impedance spectroscopy technique were generally compatible with those obtained with mercury intrusion porosimetry. It is possible to use impedance spectroscopy as a way to follow the development of the pore network in the mortars that incorporate VP as clinker replacement;
- The addition of VP, up to 20% of the binder, allowed the durability-related properties of the mortars to be improved. These improvements could be linked to the more refined microstructure produced by the pozzolanic activity of VP;
- The addition of 10% volcanic powder did not present losses in the compressive strength of the mortars, fulfilling the compressive strength requirements of the corresponding standard;
- From the results obtained in this study, it has been noted that the mortars that incorporate 10% or 20% VP as a clinker replacement showed good service properties at high hardening times (400'days), even exceeding the properties of the CEM I control mortars;
- From an environmental point of view, the proposed material is attractive since it makes use of VP, in this way, avoiding or reducing the harmful effects in the short term that VP could produce in the natural soil on which it is deposited. In addition, the potential of this replacement was shown to reduce the total greenhouse gas emissionsup to 18.66%, when 20% of CEM I is replaced by VP;
- Volcanic powder as a raw material reduces the energy costs related to mortar production, which in addition to reducing CO_2 emissions, could also reduce costs. However, this must be proven in future studies.

Author Contributions: Conceptualization, V.L., J.M.O., M.Á.C and I.S.; Data curation, J.M.O., R.M.T., I.F., T.R.-H., G.M. and M.Á.C; Formal analysis, V.L., J.M.O., R.M.T., B.I.H.-J., I.F., T.R.-H. and M.Á.C; Funding acquisition, V.L., J.M.O. and M.Á.C; Investigation, V.L., J.M.O., R.M.T., B.I.H.-J., I.F., T.R.-H. and G.M.; Methodology, V.L., J.M.O.,

R.M.T., T.R.-H., M.Á.C and I.S.; Supervision, J.M.O., M.Á.C and I.S.; Writing – original draft, V.L. and R.M.T.; Writing – review and editing, J.M.O.. The results included in this paper regarding the effects at initial hardening ages of volcanic powder addition in the studied mortars are part of the work developed along a research stay of V.L. at the University of Alicante, under the supervision of J.M.O., I.S. and M.Á.C. The results included in this paper related to the influence in the short- and long-term of the abovementioned addition, have been obtained in the PhD thesis carried out by R.M.T. at University of Alicante (Spain), under the supervision of J.M.O. and T.R.-H. All authors have read and agree to the published version of the manuscript.

Funding: This research was funded by the Universidad de La Frontera (Chile) (grant code DI19-0019, project entitled "Desarrollo de una dosificación de morteros con baja conductividad térmica para utilizar en prefabricados"), by the Conselleria de Educación, Investigación, Cultura y Deporte (at present renamed as Conselleria de Innovación, Universidades, Ciencia y Sociedad Digital) de la Generalitat Valenciana (Spain) (grant code GV/2019/070), by the Spanish Agencia Estatal de Investigación (grant code BIA2016-80982-R) and by the European Regional Development Fund (grant code BIA2016-80982-R).

Acknowledgments: Authors wish to thank Cementos Portland Valderrivas S.A. for providing the ordinary Portland cement used in this study.

Conflicts of Interest: The authors declare no conflict of interest.

References

1. Hossain, M.U.; Xuan, D.; Poon, C.S. Sustainable management and utilisation of concrete slurry waste: A case study in Hong Kong. *Waste Manag.* **2017**, *61*, 397–404. [CrossRef]
2. Labbaci, Y.; Labbaci, B.; Abdelaziz, Y.; Mekkaoui, A.; Alouani, A. The use of the volcanic powders as supplementary cementitious materials for environmental-friendly durable concrete. *Constr. Build. Mater.* **2017**, *133*, 468–481. [CrossRef]
3. Ortega, J.M.; Sánchez, I.; Climent, M.A. Influence of environmental conditions on durability of slag cement mortars. In Proceedings of the 2nd International Conference on Sustainable Construction Materials and Technologies, Ancona, Italy, 28–30 June 2010.
4. Ghanbari, M.; MonirAbbasi, A.; Ravanshadnia, M. Economic and Environmental Evaluation and Optimal Ratio of Natural and Recycled Aggregate Production. *Adv. Mater. Sci. Eng.* **2017**, *2017*. [CrossRef]
5. Ortega, J.M.; Esteban, M.D.; Rodríguez, R.R.; Pastor, J.L.; Ibanco, F.J.; Sánchez, I.; Climent, M.A. Influence of Silica Fume Addition in the Long-Term Performance of Sustainable Cement Grouts for Micropiles Exposed to a Sulphate Aggressive Medium. *Materials* **2017**, *10*, 890. [CrossRef] [PubMed]
6. Ortega, J.M.; Letelier, V.; Solas, C.; Moriconi, G.; Climent, M.Á.; Sánchez, I. Long-term effects of waste brick powder addition in the microstructure and service properties of mortars. *Constr. Build. Mater.* **2018**, *182*, 691–702. [CrossRef]
7. Letelier, V.; Ortega, J.M.; Muñoz, P.; Tarela, E.; Moriconi, G. Influence of Waste brick powder in the mechanical properties of recycled aggregate concrete. *Sustainability* **2018**, *10*, 1037. [CrossRef]
8. Medina, C.; Banfill, P.F.G.; Sánchez de Rojas, M.I.; Frías, M. Rheological and calorimetric behaviour of cements blended with containing ceramic sanitary ware and construction/demolition waste. *Constr. Build. Mater.* **2013**, *40*, 822–831. [CrossRef]
9. Celik, K.; Meral, C.; Gursel, A.P.; Mehta, P.K.; Horvath, A.; Monteiro, P.J.M. Cement & Concrete Composites Mechanical properties, durability, and life-cycle assessment of self-consolidating concrete mixtures made with blended portland cements containing fly ash and limestone powder. *Cem. Concr. Compos.* **2015**, *56*, 59–72. [CrossRef]
10. Cordeiro, G.C.; Toledo Filho, R.D.; Tavares, L.M.; Fairbairn, E.M.R. Experimental characterization of binary and ternary blended-cement concretes containing ultrafine residual rice husk and sugar cane bagasse ashes. *Constr. Build. Mater.* **2012**, *29*, 641–646. [CrossRef]
11. Huntzinger, D.N.; Eatmon, T.D. A life-cycle assessment of Portland cement manufacturing: Comparing the traditional process with alternative technologies. *J. Clean. Prod.* **2009**, *17*, 668–675. [CrossRef]
12. Stafford, F.N.; Raupp-pereira, F. Life cycle assessment of the production of cement: A Brazilian case study. *J. Clean. Prod.* **2016**, *137*, 1293–1299. [CrossRef]
13. Rajamma, R.; Senff, L.; Ribeiro, M.J.; Labrincha, J.A.; Ball, R.J.; Allen, G.C.; Ferreira, V.M. Biomass fly ash effect on fresh and hardened state properties of cement based materials. *Compos. Part B Eng.* **2015**, *77*, 1–9. [CrossRef]

14. Güneyisi, E.; Gesoğlu, M.; Akoi, A.O.M.; Mermerdaş, K. Combined effect of steel fiber and metakaolin incorporation on mechanical properties of concrete. *Compos. Part B Eng.* **2014**, *56*, 83–91. [CrossRef]
15. Pastor, J.L.; Ortega, J.M.; Flor, M.; López, M.P.; Sánchez, I.; Climent, M.A. Microstructure and durability of fly ash cement grouts for micropiles. *Constr. Build. Mater.* **2016**, *117*. [CrossRef]
16. Ortega, J.M.; Pastor, J.L.; Albaladejo, A.; Sánchez, I.; Climent, M.A. Durability and compressive strength of blast furnace slag-based cement grout for special geotechnical applications. *Mater. Constr.* **2014**, *64*. [CrossRef]
17. Ortega, J.M.; Ferrandiz, V.; Antón, C.; Climent, M.A.; Sánchez, I. Influence of curing conditions on the mechanical properties and durability of cement mortars. In *Materials Characterisation IV: Computational Methods and Experiments*; Mammoli, A.A., Brebbia, C.A., Eds.; WIT Press: Southampton, UK, 2009; pp. 381–392. [CrossRef]
18. Naceri, A.; Hamina, M.C. Use of waste brick as a partial replacement of cement in mortar. *Waste Manag.* **2009**, *29*, 2378–2384. [CrossRef]
19. Siddique, R. Properties of concrete made with volcanic ash. *Resour. Conserv. Recycl.* **2012**, *66*, 40–44. [CrossRef]
20. Habert, G.; Choupay, N.; Montel, J.M.; Guillaume, D.; Escadeillas, G. Effects of the secondary minerals of the natural pozzolans on their pozzolanic activity. *Cem. Concr. Res.* **2008**, *38*, 963–975. [CrossRef]
21. SeddikMeddah, M. Durability performance and engineering properties of shale and volcanic ashes concretes. *Constr. Build. Mater.* **2015**, *79*, 73–82. [CrossRef]
22. Hossain, K.M.A.; Lachemi, M. Strength, durability and micro-structural aspects of high performance volcanic ash concrete. *Cem. Concr. Res.* **2007**, *37*, 759–766. [CrossRef]
23. Kupwade-Patil, K.; Al-Aibani, A.F.; Abdulsalam, M.F.; Mao, C.; Bumajdad, A.; Palkovic, S.D.; Büyüköztürk, O. Microstructure of cement paste with natural pozzolanic volcanic ash and Portland cement at different stages of curing. *Constr. Build. Mater.* **2016**, *113*, 423–441. [CrossRef]
24. Kupwade-Patil, K.; Palkovic, S.D.; Bumajdad, A.; Soriano, C.; Büyüköztürk, O. Use of silica fume and natural volcanic ash as a replacement to Portland cement: Micro and pore structural investigation using NMR, XRD, FTIR and X-ray microtomography. *Constr. Build. Mater.* **2018**, *158*, 574–590. [CrossRef]
25. Anwar Hossain, K.M. Performance of volcanic ash based precast and in situ blended cement concretes in marine environment. *J. Mater. Civ. Eng.* **2005**, *17*, 694–702. [CrossRef]
26. Hossain, K.M.A. Blended cement using volcanic ash and pumice. *Cem. Concr. Res.* **2003**, *33*, 1601–1605. [CrossRef]
27. Kupwade-Patil, K.; de Wolf, C.; Chin, S.; Ochsendorf, J.; Hajiah, A.E.; Al-Mumin, A.; Büyüköztürk, O. Impact of Embodied Energy on materials/buildings with partial replacement of ordinary Portland Cement (OPC) by natural Pozzolanic Volcanic Ash. *J. Clean. Prod.* **2018**, *177*, 547–554. [CrossRef]
28. Romero, J.E.; Morgavi, D.; Arzilli, F.; Daga, R.; Caselli, A.; Reckziegel, F.; Viramonte, J.; Díaz-Alvarado, J.; Polacci, M.; Burton, M.; et al. Eruption dynamics of the 22–23 April 2015 Calbuco Volcano (Southern Chile): Analyses of tephra fall deposits. *J. Volcanol. Geotherm. Res.* **2016**, *317*, 15–29. [CrossRef]
29. Reckziegel, F.; Bustos, E.; Mingari, L.; Báez, W.; Villarosa, G.; Folch, A.; Collini, E.; Viramonte, J.; Romero, J.; Osores, S. Forecasting volcanic ash dispersal and coeval resuspension during the April–May 2015 Calbuco eruption. *J. Volcanol. Geotherm. Res.* **2016**, *321*, 44–57. [CrossRef]
30. Asociación Española de Normalización y Certificación (AENOR). *UNE-EN 197-1:2011. Composición, Especificaciones y Criterios de Conformidad de Los Cementos Comunes*; AENOR: Madrid, Spain, 2011; p. 30. (In Spanish)
31. Asociación Española de Normalización y Certificación (AENOR). *UNE-EN 196-1:2005. Métodos de Ensayo de Cementos. Parte 1: Determinación de Resistencias Mecánicas*; AENOR: Madrid, Spain, 2005; p. 36. (In Spanish)
32. Fraj, A.B.; Idir, R. Concrete based on recycled aggregates – Recycling and environmental analysis: A case study of paris' region. *Constr. Build. Mater.* **2017**, *157*, 952–964. [CrossRef]
33. OECD Climate Change Mitigation Policies. Available online: http://www.compareyourcountry.org/climate-policies?cr=oecd\protect\T1\textbraceleft$\delimiter"026E30F$&\protect\T1\textbracerightlg=en\protect\T1\textbraceleft$\delimiter"026E30F$&\protect\T1\textbracerightpage=2\protect\T1\textbraceleft$\delimiter"026E30F$&\protect\T1\textbracerightvisited=1 (accessed on 28 July 2018).

34. Williams, M.; Ortega, J.M.; Sánchez, I.; Cabeza, M.; Climent, M.A. Non-Destructive Study of the Microstructural Effects of Sodium and Magnesium Sulphate Attack on Mortars Containing Silica Fume Using Impedance Spectroscopy. *Appl. Sci.* **2017**, *7*, 648. [CrossRef]
35. Cabeza, M.; Merino, P.; Miranda, A.; Nóvoa, X.R.; Sanchez, I. Impedance spectroscopy study of hardened Portland cement paste. *Cem. Concr. Res.* **2002**, *32*, 881–891. [CrossRef]
36. Cabeza, M.; Keddam, M.; Nóvoa, X.R.; Sánchez, I.; Takenouti, H. Impedance spectroscopy to characterize the pore structure during the hardening process of Portland cement paste. *Electrochim. Acta* **2006**, *51*, 1831–1841. [CrossRef]
37. Ortega, J.M.; Sánchez, I.; Climent, M.A. Impedance spectroscopy study of the effect of environmental conditions in the microstructure development of OPC and slag cement mortars. *Arch. Civ. Mech. Eng.* **2015**, *15*, 569–583. [CrossRef]
38. Macdonald, J.B.; Johnson, W. Impedance Spectroscopy: Theory, Experiment, and Applications. In *Impedance Spectroscopy: Theory, Experiment, and Applications*, 2nd ed.; John Wiley & Sons, Inc.: Hoboken, NJ, USA, 2005; pp. 1–26. ISBN 9780471716242.
39. Vladikova, D.; Zoltowski1, P.; Makowska, E.; Stoynov1, Z. Selectivity study of the differential impedance analysis—Comparison with the complex non-linear least-squares method. *Electrochim. Acta* **2002**, *47*, 2943–2951. [CrossRef]
40. Asociación Española de Normalización y Certificación (AENOR). *UNE 83982:2008. Durabilidad del Hormigón. Métodos de Ensayo. Determinación de La Absorción de Agua Por Capilaridad del Hormigón Endurecido. Método Fagerlund*; AENOR: Madrid, Spain, 2008; p. 8. (In Spanish)
41. Ortega, J.M.; Sánchez, I.; Antón, C.; de Vera, G.; Climent, M.A. Influence of environment on durability of fly ash cement mortars. *ACI Mater. J.* **2012**, *109*, 647–656.
42. Rilem recommendation TC 116-PCD. Permeability of concrete as a criterion of its durability. *Mater. Struct.* **1999**, *32*, 174–179.
43. Andrade, C.; Alonso, C.; Arteaga, A.; Tanner, P. Methodology based on the electrical resistivity for the calculation of reinforcement service life. In Proceedings of the 5th CANMET/ACI International Conference on Durability of Concrete, Supplementary Papers, Barcelona, Spain, 4–9 June 2000; Malhotra, V.M., Ed.; American Concrete Institute: Farmington Hills, MI, USA, 2000; pp. 899–915.
44. American Society for Testing and Materials (ASTM). *ASTM C1202-12, Standard Test Method for Electrical Indication of Concrete's Ability to Resist Chloride Ion Penetration*; ASTM International: West Conshohocken, PA, USA, 2012; p. 8.
45. Nordtest. *NT Build 492. Concrete, Mortar and Cement-Based Repair Materials: Chloride Migration Coefficient from Non-Steady-State Migration Experiments*; Nordtest Espoo: Greater Helsinki, Finland, 1999; p. 8.
46. Hammond, G.P.; Jones, C.I. Embodied energy and carbon in construction materials. *Proc. Inst. Civ. Eng. Energy* **2008**, *161*, 87–98. [CrossRef]
47. Letelier, V.; Ortega, M.; Tarela, E.; Muñoz, P.; Henríquez-Jara, B.I.; Moriconi, G. Mechanical Performance of Eco-Friendly Concretes with Volcanic Powder and Recycled Concrete Aggregates. *Sustainability* **2018**, *10*, 3036. [CrossRef]
48. UK Government. Department for Business, E. & I. S. Government Emission Conversion Factors for Greenhouse Gas Company Reporting. Available online: https://www.gov.uk/government/collections/government-conversion-factors-for-company-reporting (accessed on 7 August 2018).
49. Liu, Y.; Sidhu, K.S.; Chen, Z.; Yang, E.-H. Alkali-treated incineration bottom ash as supplementary cementitious materials. *Constr. Build. Mater.* **2018**, *179*, 371–378. [CrossRef]